Structural Chemistry (2018) 29:1709–1721
https://doi.org/10.1007/s11224-018-1152-y

ORIGINAL RESEARCH

A mechanistic MEDT study of the competitive catalysed [4+2] and [2+2] cycloaddition reactions between 1-methyl-1-phenylallene and methyl acrylate: the role of Lewis acid on the mechanism and selectivity

Leila Barama[1] · Brahim Bayoud[1] · Fouad Chafaa[1,2] · Abdelmalek Khorief Nacereddine[1,3] · Abdelhafid Djerourou[1]

Received: 28 April 2018 / Accepted: 25 June 2018 / Published online: 3 July 2018

Abstract

The selectivity and the nature of the mechanism of the competitive Lewis acid catalysed [4+2]/[2+2] cycloaddition reactions of 1-methyl-1-phenylallene (**MPA**) with methylacrylate (**MA**) have been theoretically studied within the Molecular Electron Density Theory using DFT methods at the B3LYP/6-31G(d) theoretical level. DFT reactivity indices indicate that **MPA** is a strong nucleophile and the **LA-MA** complex is a strong electrophile. The coordination of **LA** to **MA** enhances the reaction rate and increases the asynchronicity of the [4+2] CA reaction, changes the nature of the mechanism from one step to stepwise for the [2+2] CA reaction and increases the polar character of these cycloaddition reactions, which become demands a relatively low activation energy. Analysis of different energy profiles indicates that these competitive LA-catalysed CA reactions favour the formation of a mixture of *meta* regioisomers in both types of cycloaddition, in which the [4+2] cycloadducts were obtained in majority amount, in agreement with the experiment. Analysis based on Electron Localisation Function topological shows that the favoured [4+2] CA reaction takes place through a non-concerted two-stage one-step mechanism.

Keywords Cycloaddition · Mechanism · Catalyst · Selectivity · DFT calculations · ELF analysis · MEDT

Introduction

Cycloadditions are one of the most important organic reactions since they allow us to prepare both carbocyclic and heterocyclic structures with useful utilisation in medicinal and industrial fields [1]. The Diels–Alder cycloaddition is a key method for construct, in a regio- and stereocontrolled manner, six-membered rings. In addition, it represents a simple and economic synthetic tool for constructing complex molecules [2, 3]. On the other hand, [2+2] cycloadditions are mainly used to prepare four-membered cyclic compounds. The most catalytic enantioselective [2+2] cycloadditions require the use of highly polarised electron-rich and electron-poor alkenes [4–6]. The literature contains a great amount of both experimental and theoretical studies which treat the subject of mechanism and selectivities of Diels–Alder and [2+2] cycloaddition reactions [7–10]. Indeed, [2+2] cycloadditions usually proceed via a stepwise, biradical [11] or zwitterionic mechanism [12]. In addition, [4+2] cycloaddition reactions may be proceed with one-step synchronous non-polar mechanisms through a biradicaloidal transition states or through a stepwise biradical mechanism [13, 14]. In the other hand, these cycloadditions may be also occurring via a polar one-step two-stage or stepwise zwitterionic mechanism [15–17].

Recently, Conner et al. performed experimentally the Lewis acid ($AlCl_3$) catalysed Diels-Alder cycloaddition between 1-methyl-1-phenylallene and methylacrylate [18]. They have found that this cycloaddition reaction is characterised by a high regioselectivity leading to the formation of *meta* cycloadducts as a one regiocycloadduct and favour the [4+2] cycloaddition over the [2+2] one (Scheme 1). It

Electronic supplementary material The online version of this article (https://doi.org/10.1007/s11224-018-1152-y) contains supplementary material, which is available to authorized users.

✉ Abdelmalek Khorief Nacereddine
khorief.abdelmalek@univ-annaba.org

[1] Laboratoire de Synthèse et Biocatalyse Organique, Département de Chimie, Faculté des Sciences, Université Badji Mokhtar Annaba, BP 12, 23000 Annaba, Algeria

[2] Département de Chimie, Faculté des Sciences, Université Saad Dahleb Blida 1, Route de Soumâa, BP 270, 09000 Blida, Algeria

[3] Département de Physique et Chimie, Ecole Normale Supérieure d'Enseignement Technologique de Skikda, Cité des frères Boucetta, Azzaba, Skikda, Algeria

Scheme 1 Experimental $AlCl_3$ Catalysed cycloaddition reaction of **MPA** with **MA**

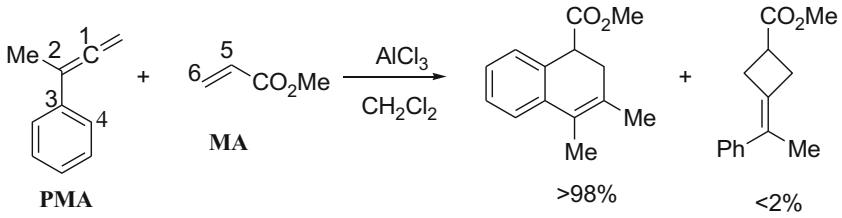

has been established that when [4+2] and [2+2] CAs reactions are in competition, some studies postulated that these cycloaddition are not independent, it proceed through the same biradical intermediate [19].

Contrariwise, some studies indicate that both types of cycloaddition proceed via completely independent channels without any common critical points [11].

Our research axis is based on the study of the mechanism and selectivities observed experimentally in cycloaddition reactions [20–24]. Therefore, herein, we undertook a theoretical investigation using transition state theory and DFT-based reactivity indices of the regio- and stereoselectivities for explaining experimentally *meta* regioselectivity performed by Conner's group [18]. Furthermore, we deepen our study by analysing the nature of molecular mechanism in order to find the factors influenced on the selectivity and understanding the role of the Lewis acid catalyst in the reactivity and selectivity of these competitive cylcoaddition reactions between **MPA** with **MA**.

Calculation details

The geometries of all structures involved in this study were first introduced by GaussView 05 [25] then full optimised using Gaussian 09 suite of program [26]. The calculation was performed using quantum chemical DFT methods at the B3LYP/6-31G (d) level of theory [27–30]. The nature of all optimised stationary points (reactants, transition states and cycloadducts) was confirmed by frequency calculations, in which only TSs has a single imaginary frequency corresponding to the new forming bonds. The effects of dichloromethane (DCM) solvent were also evaluated using the polarisable continuum model (PCM) [31, 32] within the self-consistent reaction field (SCRF) [33–35]. The thermodynamic proprieties such as enthalpies, entropies, and Gibbs free energies were computed at standard conditions; 298 K and 1 atm [36]. The electronic structures of stationary points were analysed by the natural bond orbital (NBO) method [37, 38]. The electron localisation function (ELF) topological analysis [39] was performed using Multiwfn software [40] from the B3LYP/6–31G(d) monodeterminantal wave functions of the pertinent points selected from the IRC diagram. The global electrophilicity index ω [41] is given by the expression, $\omega = \mu^2/2\eta$ focusing on the electronic chemical potential, μ, and the chemical hardness, η. These two quantities are calculated using the one-electron energies of the frontier molecular orbital HOMO and LUMO, ε_H and ε_L, as $\mu \approx (\varepsilon_H + \varepsilon_L)/2$ and $\eta \approx (\varepsilon_L - \varepsilon_H)$, respectively [42, 43]. The global nucleophilicity index *N* [44] is calculated also based on the HOMO energies [45] according the following equation, $N = \varepsilon_{HOMO\ (Nu)} - \varepsilon_{HOMO\ (TCE)}$, where, (*Nu*) indicates the nucleophile and TCE is tetracyanoethylene used as reference. The Nucleophilic and electrophilic Parr functions [46] indicating the local reactive centres of the separated reactants were extracted from the analysis of the Mulliken atomic spin density (ASD) of the radical anion of electrophile fragments **MA** and **MA-LA** complex and the radical cation of the nucleophile fragment, **MPA**.

Results and discussion

This study is structured into four parts; the first is devoted to the analysis of the DFT reactivity indices of the reagents involved in these CA reactions of **MPA** with **MA**, in order to determine the electronic character and the regioselectivity of the reaction. The second part is dedicated to the exploration and characterisation of the energy profiles of the non-catalysed and Lewis acid catalysed [4+2] and [2+2] CA reactions between **MPA** and **MA**. At the last part, we placed an ELF topological analysis corresponding to the formation of the new C1–C6 and C4–C5 single bonds of the most favoured *meta* channel of the [4+2] CA reaction between **MPA** and **MA**.

DFT-based reactivity indices analysis

Global indices

The values of the global indices, namely, electronic chemical potentials (μ), the global electrophilicity indices (ω), the

Table 1 FMO energies and values of global reactivity indices, in eV, of **MPA**, **MA** and **MA-LA** complex

	HOMO	LUMO	μ	η	ω	N
MPA	− 5.85	− 0.63	− 3.24	5.22	1.01	3.27
MA	− 7.35	− 1.25	− 4.30	6.11	1.51	1.77
MA-LA	− 7.75	− 3.17	− 5.46	4.58	3.25	1.37

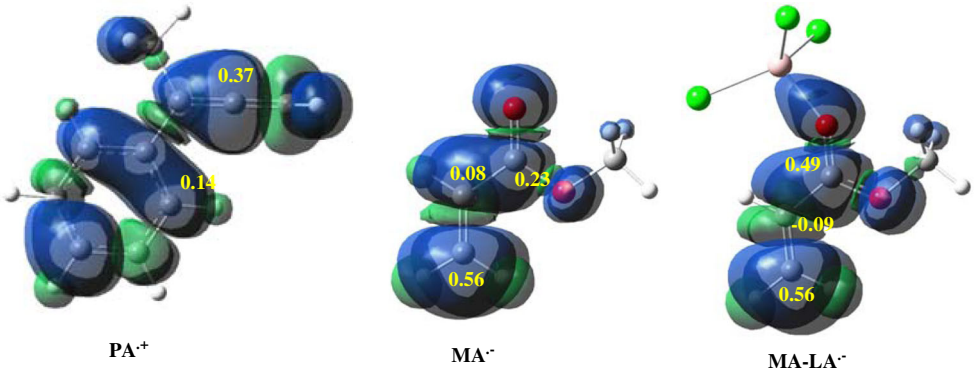

Fig. 1 Maps of ASD representation of the radical cation **MPA**$^{\bullet+}$and the radical anions **MA**$^{\bullet-}$ and **MA-C**$^{\bullet-}$ with local Parr indices of the most reactive atoms for **MPA**, **MA** and **MA-LA** molecular systems

chemical hardness (η) and the global nucleophilicity indices *N* of the separated reagents **MPA**, **MA** and the corresponding Lewis acid coordinated complexes **MA-LA** are calculated using the above relations and collected in Table 1.

A comparison between the electronic chemical potential (μ) values shows that the **MPA** presents a highest values (− 3.24 eV) than that of **MA** (− 4.30 eV) and the **MA-LA** (− 5.46), indicating that the flux of global electron density transfer (GEDT) will take place from **MPA** towards **MA** or **MA-LA**. Therefore, the **MPA** will react as a nucleophile, whereas, both **MA** and **MA-LA** are considered as an electrophilic reagents. Moreover, the global electrophilicity index value of **MA** (1.51 eV) is higher than that of **MPA** (1.01 eV). This high value indicates that this ethylenic species is classified according to the absolute scale of electrophilicity [47] on the borderline of moderate electrophile. Coordination of Lewis acid $AlCl_3$ to the carbonyl oxygen atom of the **MA** will increase dramatically the electrophilicity of this ethylene towards 3.25 eV, and thereby become a strong electrophile, which explain the decrease of the activation energy and increase the polar character of these CA reactions (see latter). On the other hand, the global nucleophilicity indices of the **MPA**, **MA** and **MA-LA** confirm that **MPA** is a good nucleophile, whereas, **MA** and **MA-LA** complex are a bad nucleophiles. The low electorphilicity difference between the **MPA** and **MA** (Δω = 0.50 eV) indicates for high activation energy and the low polar character of this CA reaction. However, the coordination of Lewis acid to the **MA** (**MA-LA**) increases considerably this difference to become 2.24 eV, explaining both low activation energy and the high polar character of the associated CA reaction.

Table 2 Relative energies, in gas phase and in dichloromethane solution of the TSs and CAs involved in the non-catalysed [4+2] CA reaction of **MPA** with **MA**

System	$\Delta E_{\text{Gas phase}}$ (kcalmol^{-1})	$\Delta E_{\text{Dichloromethane}}$ (kcalmol^{-1})
TS1mn	22.64	22.21
TS1mx	22.36	22.22
TS1on	29.98	30.31
TS1ox	30.51	31.33
CA1mn	− 28.55	− 12.90
CA1mx	− 30.36	− 14.62
CA1on	− 13.60	− 13.13
CA1ox	− 13.11	− 12.45

Local indices

To predict the regioselectivity of these competitive CA reactions, recent studies indicate that the most favourable reactive channel is that implied the most two-centre interaction which occur between the most electrophilic centre of the electrophile and the most nucleophilic centre of the nucleophile [48–53]. Recently, Domingo and co-workers [46] discovered a new method based on the electrophilic and nucleophilic Parr functions P^+_k and P^-_k, respectively, which are obtained from the changes of spin electron density, occurred via the GEDT process. This method proved to be a powerful tool for the study of the local reactivity, and thereby, determine the observed experimental regioselectivity.

The maps of the Atomic Spin Density (ASD) of these systems, the radical cation of **MPA** and the radical anions of **MA** and **MA-LA** complex, together with the values of nucleophilic Parr indices of **MPA** and the electrophilic Parr indices of **MA** and **MA-C** are given in Fig. 1.

From Fig. 1, analyses of nucleophilic Parr indices of **MPA** indicate that the C1 carbon atom (see Scheme 1 for atom numbering) is the most nucleophilic centre of this nucleophile, $P^-_{C1} = 0.37$. On the other hand, the electrophilic Parr indices of **MA** and **MA-LA** complex are mainly concentrated at the C6 carbon atom $P^-_{C6} = 0.56$ for both electrophilic systems. Coordination of Lewis acid to **MA** does not modify the electrophilicity index of the C6 atom but it decrease that of C5 by moving it into the carbonyl function. Therefore, the present CA reactions leading to the formation of the cycloadduct generated from the interaction between C1 carbon atom of the **MPA** and the C6 one of **MA** and **MA-LA**, justifying the total *meta* regioselectivity for both [4+2] or [2+2] CA reactions, in agreement to the experimental observations [18].

Scheme 2 The possible regio- and stereoisomeric pathways for the [4+2] CA reaction between **MPA** and **MA**

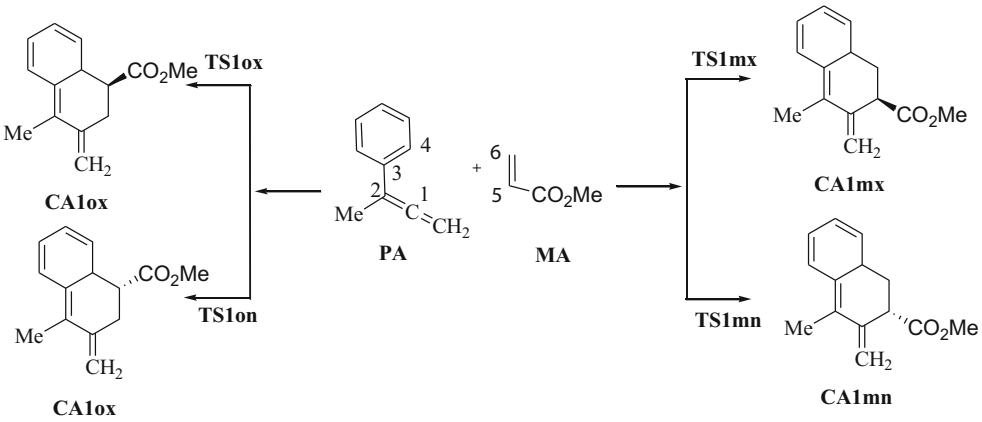

Energy profiles and geometries analysis

Non-catalysed [4+2] CA reaction

Energies Table 2 shows the values of the relative energies of the TSs and CAs corresponding to the [4+2] CA reaction between **MPA** and **MA**, in gas phase and in solution of dichloromethane, while total ones are given in Table S1 in Supporting Information. Owing to the asymmetry of both reactants, the [4+2] CA reactions of **MPA** with **MA** could take place along four reactive channels (see Scheme 2). The *endo* and *exo* nomenclatures are related to the two stereoisomeric approach modes of the methoxycarbonyle group of the **MA** towards the C1=C2–C3=C4 diene system of **MPA**. Therefore, along the *endo* approach, the methoxycarbonyle group is directed towards the diene system of the **MPA** framework, and for the *exo* approach is the opposite. The possible *ortho* and *meta* regioisomeric channels are corresponding to the interaction modes of the C5 or C6 carbon atoms of **MA** with the **MPA** C1 carbon, in such a manner that this last interact with C5 carbon atom along the *ortho* reactive pathway.

The analysis through IRC paths, which connected the TSs to its two minimums, indicated that the non-catalysed [4+2] reactions of **MPA** with **MA** take place through a one-step mechanism. Thereby, in addition to the separated reactants, we have located and characterised four TSs and the corresponding four cycloadducts (CAs) for this CA reaction.

Table 3 Relative enthalpies (ΔH, in kcal mol^{-1}), relative entropies (ΔS, in cal·mol^{-1} K^{-1}), and relative free energies (ΔG, in kcal mol^{-1}), of for TSs and CAs involved in the non-catalysed [4+2] CA reaction between **MPA** and **MA**

System	ΔH	ΔS	ΔG
TS1ox	31.81	−48.949	46.25
TS1on	30.76	−49.146	45.27
TS1mx	22.69	−46.421	36.39
TS1mn	22.70	−45.026	35.99
CA1ox	−9.45	−51.311	5.70
CA1on	−10.16	−51.802	5.12
CA1mx	−11.59	−48.774	2.80
CA1mn	−9.85	−50.291	4.99

From Table 2, the comparison between the activation energies of all reactive pathways indicates that the *meta* regioisomers is kinetically favoured than the *ortho* ones by about 8 $kcalmol^{-1}$, in which the *meta exo* approach is slightly more favoured than the *meta-endo* one. On the other hand, the *meta* cycloadducts are more stable than the *ortho* ones. Therefore, the *ortho* reactive pathways are unfavourable both kinetically and thermodynamically; in greet agreement with experimental data.

In order to deepen our analysis of the energetic reaction profiles, we have included the effect of solvent-solute interactions along the reaction pathways. A comparison between the gas phase energy values and these of the dichloromethane shows that the activation energies decrease very slightly for the *meta* approaches and increase for the *ortho* ones, and remains the *meta* approaches the most favoured regioisomeric pathways.

Since the most organic reactions occurs in solution and demands an energetic enhancing such as heating or radiation, and these factors may be influenced on the energy values, a thermodynamic analysis of enthalpy, entropy, and free energy become necessary. Values of relative enthalpies, entropies, and Gibbs free energies of the stationary points involved in the [4+2] CA reaction of **MPA** with **MA** are displayed in Table 3, while total ones are given in Table S2 in Supporting Information.

Inclusion of thermal corrections to the electronic energies increases slightly the relative enthalpies by about 0.1 kcal mol^{-1} (see Table 3), in which the *meta* pathways are remaining more favourable than the *ortho* ones by about 8 kcal mol^{-1}, demonstrating that these reactive pathways are characterised by an exothermic character. Addition of entropic contribution to enthalpies increases the Gibbs free energies by 13.29, 13.70, 14.51, and 14.44 kcal mol^{-1} for **TS1on**, **TS1ox**, **TS1mn**, and **TS1mx**, respectively. This increases is due to the unfavourable entropies associated with this bimolecular process, the reaction being endergonic by between 2.80 and 5.70 kcal mol^{-1}. Analysis of the Gibbs free energies indicates that this [4+2] CA reaction between **MPA** and **MA** is rather unfavourable,

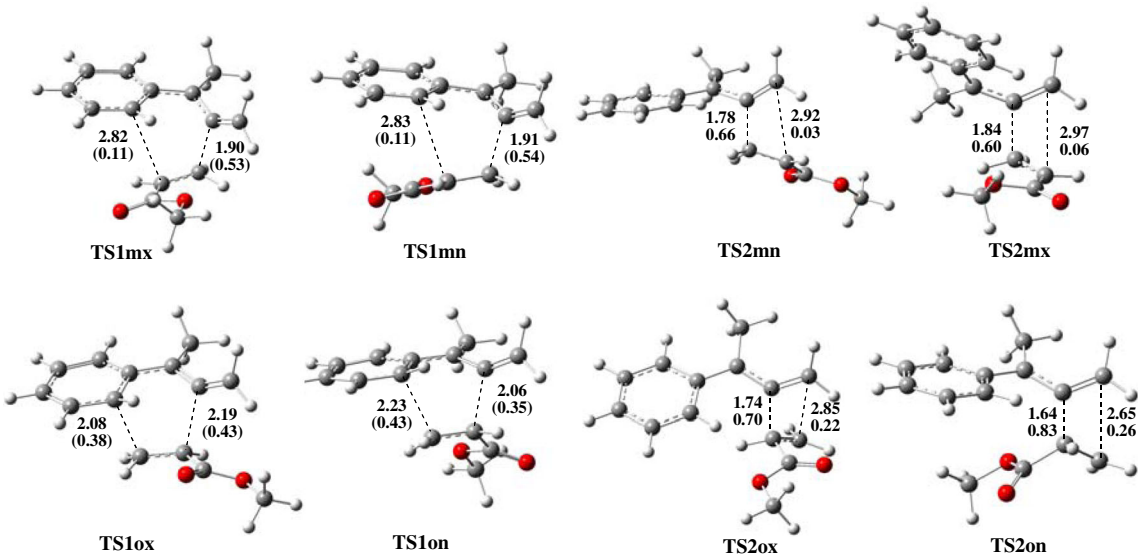

Fig. 2 Optimised Geometries of the TSs associated with the non-catalysed [4+2] and [2+2] CAs reaction between **MPA** and **MA** including the lengths of the new forming bonds in Å and Wiberg indices between brackets

having an activation Gibbs free energy of 35.99 kcal mol^{-1} for the more favourable **TS1mn** and being slightly endergonic, which accounts for the reversibility of this [4+2] CA reaction, thereby, the use of a Lewis acid for reducing the activation energies is required for the feasibility of this CA reaction.

Geometries analysis The optimised geometries of the TSs associated with the non-catalysed [4+2] CA reaction of **MPA** with **MA** are given in Fig. 2. At the *meta* TSs, the distances C1… C6, and C4…C5 of the C1–C6 and C4–C5 single new forming bonds are 1.90 and 2.83 Å at **TS1mn** and 1.90 and 1.82 Å at **TS1mx**, respectively, while at the *ortho* TSs, the distances between C1…C5 and C4…C6 of the corresponding new single bonds are 2.06 and 2.23 Å at **TS1on** and 2.19 and 2.08 Å at **TS1ox**. Therefore, the new C−C single bonds at the most favourable *meta* TSs take place through an asynchronous bond formation processes, in which the formation of C1−C6 single bond is more advanced than the C4−C5 one, while for the *ortho* TSs is slightly synchronous. These remarks have been confirmed by the values of Wiberg bond indices [54] (see Fig. 2).

The electronic nature of the non-catalysed [4+2] CA reaction of **MPA** with **MA** was evaluated by calculating the value of GEDT [55] at all transition states. The values of the GEDT computed at the **MA** moiety of the TSs are 0.13e at **TS1mn**, 0.12e at **TS1mx**, 0.05e at **TS1on** and 0.06e at **TS1ox**. These low values indicate that the [4+2] CA reaction of **MPA** with **MA** has a low polar character, in agreement with the analysis of the global reactivity indices and with the obtained high activation energy for this CA reaction.

Non-catalysed [2+2] CA reaction

Energies In this part, the second competitive non-catalysed [2+2] CA reaction of **MPA** with **MA** is also studied (see Scheme 3). Relative energies of the TSs and CAs involved in this [2+2] CA reaction, in gas phase and in dichloromethane solution are gathered in Table 4, while total ones are given in Table S3, in Supporting Information.

The gas phase activation energies associated with the four reactive channels of this CA reaction are 24.69 (**TS2mn**), 23.46 (**TS2mx**), 40.10 (**TS2on**) and 36.33 kcal·mol^{-1}

Scheme 3 The possible regio- and stereoisomeric pathways for the non-catalysed [2+2] CA reaction between **MPA** and **MA**

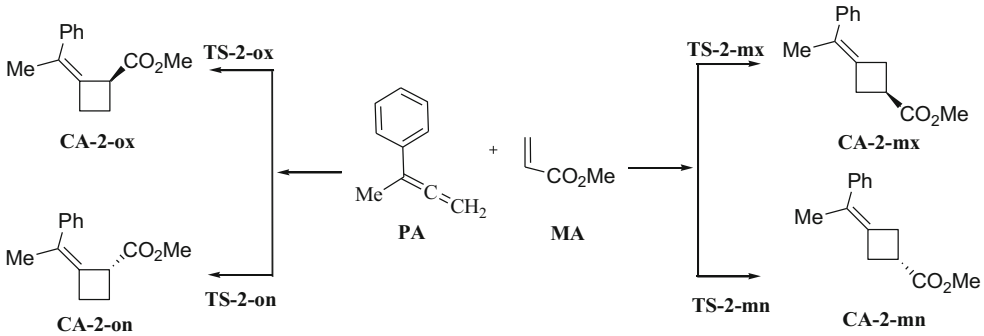

Table 4 Relative energies, in gas phase and in dichloromethane solution of for TSs and CAs involved in the non-catalysed [2+2] CA reaction of **MPA** with **MA**

System	$\Delta E_{Gas\ phase}$ (kcalmol^{-1})	$\Delta E_{Dichloromethane}$ (kcalmol^{-1})
TS2mn	24.69	23.65
TS2mx	23.46	22.75
TS2on	40.10	40.42
TS2ox	36.33	37.46
CA2mn	− 26.33	− 26.71
CA2mx	− 28.56	− 27.79
CA2on	− 26.33	− 25.77
CA2ox	− 26.36	− 25.60

(**TS2ox**), the reaction being exothermic by 26.33 (**CA2mn**), 28.56 (**CA2mx**), 26.33 (**CA2on**) and 26.36 kcal mol^{-1} (**CA2mx**). The high exothermic character of this CA reaction makes these [2+2] CA reaction pathways irreversible in gas phase. The activation energy of the most favourable *meta/exo* approach via **TS2mx** (23.46 kcal mol^{-1}) is 12.87 kcal mol^{-1} lower than that associated with the most favoured stereoisomeric *ortho/exo* one via **TS2ox**. This high energy difference indicates that the non-catalysed [2+2] CA reaction between **MPA** and **MA** is completely *meta* regiospecific, yielding *meta* regioisomeric [2+2] CAs, in good agreement with the analysis of local indices and experimental observations.

Taking account that this CA reaction was carried out in dichloromethane solution, which can have some influence on the values of energies and geometries of stationery points, thereby, solvent effects were also studied. Inclusion of dichloromethane effects decreases slightly the gas phase activation energies by 1.04 (**TS2mn**), 0.71 kcal mol^{-1}(**TS2mx**), and increase it by 0.32 for **TS2on** and 1.13 kcal mol^{-1} for **TS2ox**. In addition, this solvent also slightly decreases the exothermic character of the reaction for all reactive pathways.

Table 5 Relative enthalpies (ΔH, in kcal mol^{-1}), entropies (ΔS, in cal·mol^{-1} K^{-1}) and Gibbs free energies (ΔG in kcal mol^{-1}), at 298.15 K and 1 atm, for TSs and CAs involved in the non-catalysed [2+2] CA between **MPA** and **MA**

System	ΔH	ΔS	ΔG
TS2mn	22.49	− 49.743	37.17
TS2mx	23.45	− 49.157	37.95
TS2on	40.28	− 50.007	55.04
TS2ox	37.38	− 48.433	51.68
CA2mn	− 24.34	− 48.059	− 10.15
CA2mx	− 24.80	− 45.612	− 11.34
CA2on	− 22.70	− 47.345	− 8.73
CA2ox	− 22.61	− 44.872	− 9.37

Although these changes in energies, solvent effects does not produce any change in the *meta* regioselectivity.

The values of the thermodynamic properties, namely, relative enthalpies, entropies and Gibbs free energies, associated with the four reactive channels of the non-catalysed [2+2] CA reaction between **MPA** and **MA** are listed in Table 5, while total ones are given in Table S4, in Supporting Information.

For the enthalpies, addition of the thermal corrections to the electronic energies did not significantly change the regioselectivity; while relative reaction enthalpies slightly decreased. For the free energies, addition of the entropic contribution to enthalpies strongly increases relative Gibbs free energies in the range of 14 kcal mol^{-1} due to the unfavourable entropies associated with this bimolecular process. Thus, the activation Gibbs free energies associated to the favourable regioisomeric approaches, **TS2mn** and **TS-2mx** reach to 37.17 and 37.95 kcal mol^{-1}, respectively. Additionally, the reaction becomes slightly exergonic by 10.15 (**CA2mn**) and 11.34 kcal mol^{-1} (**CA2mx**). These results indicate that the *meta* regioisomers will be obtains as a single regioisomers under both kinetic and thermodynamic controls. Although, analysis of the Gibbs free energies reveals that the non-catalysed [2+2] CA reaction between **MPA** and **MA** is also very unfavourable, leading to the formation of the *meta* regioisomers, in complete agreement with the experimental outcomes. Interestingly, these energy results are very similar to these obtained for the non-catalysed [4+2] CA reaction as predicted by the analysis of the conceptual DFT reactivity indices.

Geometries of TSs The geometries of the TSs associated with the non-catalysed [2+2] CA reaction between **MPA** and **MA** are shown also in Fig. 2. At the *meta* TSs, the distances between the C1 and C6 atoms of side, and C2 and C5 ones on the other side, which they involved in the formation of the C1–C6 and C2–C5 single bonds are 1.78 and 2.92 Å at **TS2mn** and are 1.84 and 2.94 Å at **TS2mx**, while at the *ortho* TSs, the distances between the corresponding atoms involved in the formation of the C1−C5 and C2−C6 single bonds are 1.64 and 2.65 Å at **TS2on** and 1.74 and 2.85 Å at **TS2ox**. Therefore, the formation of the new C−C single bonds at both *meta* and *ortho* TSs suggests a highly asynchronous bond formation processes, in which the formation of the single bond involving C1 atom is more advanced than the second one. This asynchronous mechanism has been confirmed by the analysis of Wiberg bond indices [54] (see Fig. 2).

The electronic nature of the non-catalysed [2+2] CA reaction between **MPA** with **MA** was also evaluated by calculation of the GEDT [55] at the TSs associated with the four reactive pathways. The values of the GEDT computed at the **MA** moiety of the TSs are 0.16e at **TS2mn**, 0.14e at **TS2mx**, 0.06e at **TS2on** and 0.02e at **TS2ox**. These low values indicate that the non-catalysed [2+2] CA reaction of **MPA** with **MA** has a low polar character, in agreement with the analysis of the global

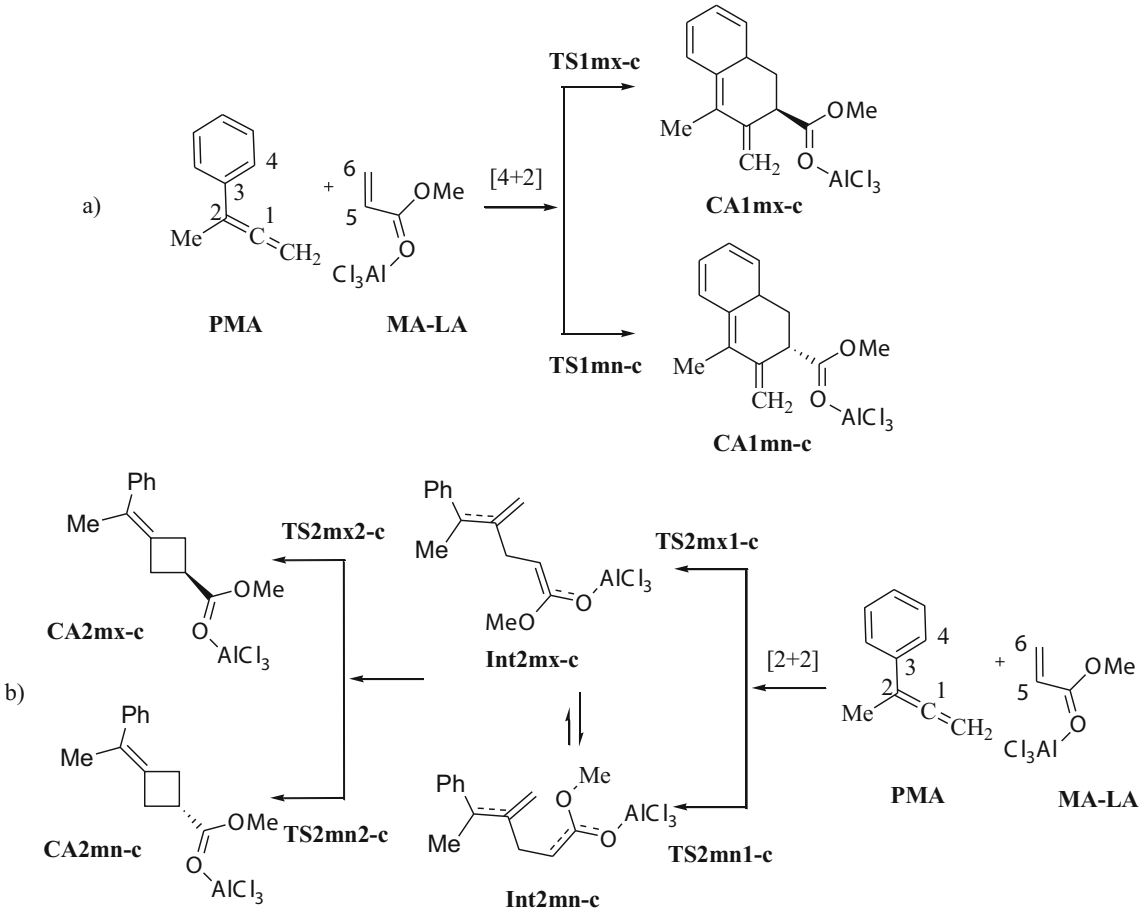

Scheme 4 The stereoselective approaches for the $AlCl_3$ catalysed [4+2] and [2+2] CA reactions for the favourable *meta* regioisomeric channel between **MPA** and **MA**

reactivity indices and with the high activation energy computed for this CA reaction.

$AlCl_3$ catalysed [4+2] and [2+2] CA reactions

Energies Coordination of the oxygen atom (C=O) of **MA** with an $AlCl_3$ catalyst notably increases its electrophilicity and enhances its reactivity towards electron-rich diene such as **MPA**. Accordingly, the Lewis acid catalysed [4+2] and [2+2] CA reactions of the **MA-LA** complex with **MPA** of the more favourable *meta* regioisomeric pathways were studied (Scheme 4). Relative energies for the TSs and cycloadducts involved in the TSs involved in the *meta* regioisomeric channel of the [4+2] and [2+2] CA reactions of **MA**-$AlCl_3$ complex with **MPA**, in the gas phase and in dichloromethane are displayed in Tables 6 and 7, while total ones are given in Table S5 and S6, respectively, in Supporting Information.

Table 6 Relative energies, in gas phase and in solvent of the TSs involved in the *meta* regioisomeric channel of the $AlCl_3$ catalysed [4+2] CA reaction of **MPA** with **MA**

System	$\Delta E_{Gas\ Phase}$ (kcalmol^{-1})	$\Delta E_{Dichloromethane}$ (kcalmol^{-1})
TS1mn-c	10.49	10.66
TS1mx-c	11.50	11.63
CA1mn-c	− 17.11	− 14.22
CA1mx-c	− 15.77	− 9.93

Table 7 Relative energies, in gas phase and in solvent of the TSs and CAs involved in the *meta* regioisomeric of the $AlCl_3$ catalysed [2+2] CA reaction of **MPA** with **MA**

System	$\Delta E_{Gas\ Phase}$ (kcalmol^{-1})	$\Delta E_{Dichloromethane}$ (kcalmol^{-1})
TS2mn-c1	13.17	13.18
TS2mx-c1	12.93	11.45
Int2mn-c	6.62	3.26
Int2mx-c	6.08	3.89
TS2mn-c2	8.17	7.36
TS2mx-c2	7.77	7.30
CA2mn-c	− 26.30	− 24.77
CA2mx-c	− 28.58	− 26.28

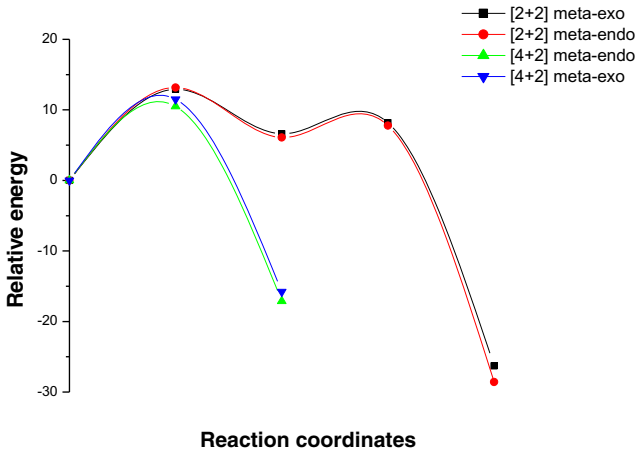

Fig. 3 Gas Phase energy profiles of the possible stereoselective pathways for the *meta* regioisomeric [4+2] and [2+2] CA reaction between **MPA** and **MA-AlCl$_3$** complex

Analysis of IRC paths of the $AlCl_3$ catalysed [4+2] CA reactions of **MPA** with **MA** indicates that this CA reaction take place through a one-step mechanism, while the [2+2] CA one proceeds via a stepwise mechanism (See Fig. 3). Thereby, six TSs and the corresponding four cycloadducts (CAs) and two intermediates were located and characterised for these competitive CA reactions (see Scheme 4).

The gas phase activation energies associated with the *meta* regioisomeric $AlCl_3$ catalysed [4+2] CA reaction are 10.49 (**TS1mn-c**) and 11.50 (**TS1mx-c**). For the comparison of [2+2] CA reaction energies with these of [4+2] CA reaction, we only considered the first step of this stepwise mechanism because it is the determining step of the reaction rate. The gas phase activation energies of this CA reaction are 13.17 (**TS2mn-c1**) and 12.93 kcalmol^{-1} for **TS2mx-c1**, thereby, a comparison between the [4+2] and [2+2] activation energies reveals that this CA reaction favour kinetically the formation of cycloadducts corresponding to the [4 + 2] processes. Furthermore, these energy results clearly indicate that with the use of the $AlCl_3$ catalyst, the activation energy decrease by 12 kcal mol^{-1}. This change makes the LA-catalysed competitive [4+2]/[2+2] CA reactions favour mostly the [4+2] reaction since it increase the energy difference to 2.44 kcalmol^{-1} between the most favoured approaches of these CA reactions, **TS1mn-c1** and **TS2mn-c1**, which has been 1.10 kcalmol^{-1} in non-catalysed processes. In addition, this energy difference suggests the formation of a mixture of both **CA1mn-c1** and **TS2mn-c1**, in which **CA1mn-c1** is the major, in a greet agreement with experimental data [18].

Inclusion of dichloromethane effects stabilises slightly the reactants, TSs and cycloadducts relative to gas phase geometries. The most remarkable change with the inclusion of solvent effects is the increase of the activation energies and the decrease of the exothermic character of the reaction. This low solvent effect can be assigned to its low polar character (μ = 1.14D).

Table 8 Relative enthalpies (ΔH in kcal mol^{-1}), relative entropies (ΔS in cal·mol^{-1} K^{-1}) and relative free energies (ΔG in kcal mol^{-1}), at 298.15 K and 1 atm, for the TSs and CAs involved in the *meta* regioisomeric channel of the LA-catalysed meta [4+2] CA between **MPA** and **MA**

	ΔH	ΔS	ΔG
TS1mn	11.91	− 39.756	23.65
TS1mx	12.91	− 39.048	24.43
CA1mn	− 6.32	− 44.457	6.80
CA1mx	− 11.01	− 50.153	3.79

Table 9 Relative enthalpies (ΔH in kcal mol^{-1}), entropies (ΔS in cal·mol^{-1} K^{-1}) and free energies (ΔG in kcal mol^{-1}), at 298.15 K and 1 atm, for the TSs and CAs involved in the *meta* regioisomeric channel of the $AlCl_3$-catalysed [2+2] CA between **MPA** and **MA**

	ΔH	ΔS	ΔG
TS2mn-c1	13.75	− 42.681	26.35
TS2mx-c1	13.07	− 48.265	27.32
Int2mn-c	5.27	− 47.410	19.26
Int2mx-c	6.51	− 42.653	19.10
TS2mn-c2	8.87	− 50.770	23.85
TS2mx-c2	8.72	− 50.289	23.56
CA1mn-c	− 23.30	− 40.240	− 11.43
CA1mx-c	− 22.97	− 53.614	− 7.14

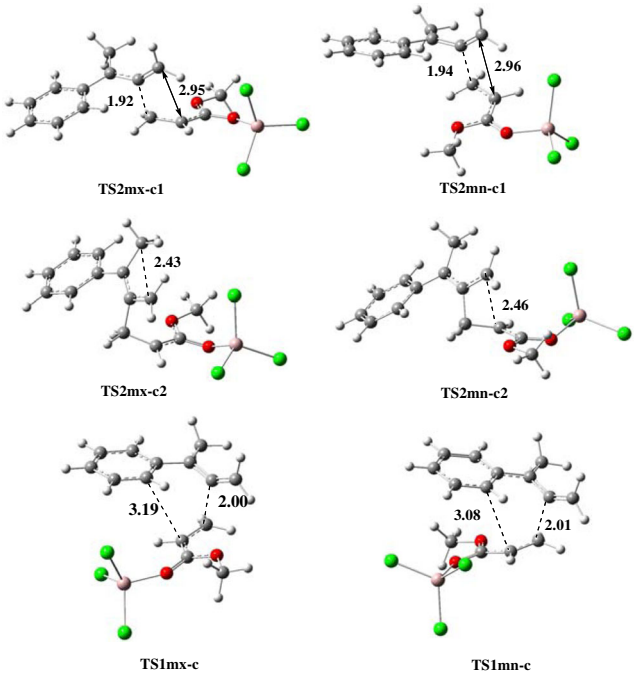

Fig. 4 Geometries of the TSs of the favourable *meta* regioisomeric [2+2] and [4+2] CA reactions between **MPA** and **MA-LA** complex including the lengths of the new forming bonds in Å

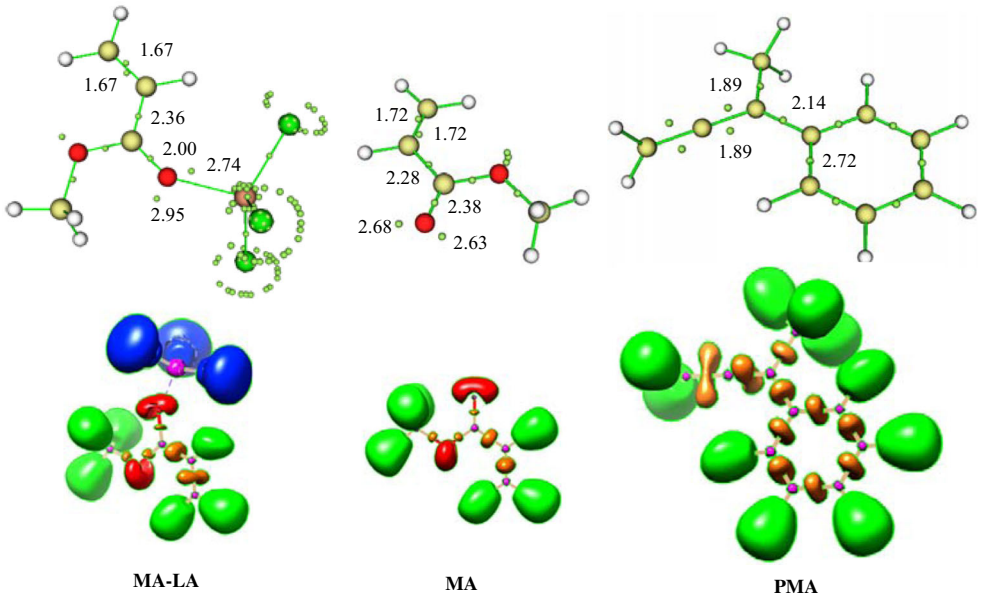

Fig. 5 ELF localisation domains, represented with an isosurface value of ELF = 0.83 and ELF basin attractor positions, together with the most representative valence basin populations of **MPA**, **MA** and **MA-LA** complex

The values relative enthalpies, entropies and free energies associated to the *meta* regioisomeric [4+2] and [2+2] CA reactions are collected in Tables 8 and 9, while, total ones are collected in Table S7 and S8, respectively in Supporting Information.

From a comparison between the activation enthalpy values, we can notice a remarkable preference for the [4+2] *meta–endo* pathway in agreement with the predicted activation energy. The high negative values of the relative entropy indicate that these CA reactions are entropically unfavourable due to the geometry voluminous of both TSs and cycloadducts and the intermolecular process of these CA reactions. Thus, the addition of the entropic contribution to the enthalpy increases the free activation energy by about 11 kcal mol^{-1}. In addition, all these reactive pathways are characterised by an exothermic character. On the other hand, the values of the free energy of the CAs account for the endergonic character of [4+2] process and the exergonic for the [2+2] pathways. Thereby, the formation of the [4+2] CAs occurs under kinetic control, whereas, the [2+2] ones is under thermodynamic control.

Geometries The optimised geometries of the TSs involved in the competitive $AlCl_3$ catalysed [4+2] and [2+2] CA reactions between **MPA** and **MA** are given in Fig. 4.

The lengths of the new forming bonds corresponding to the [4+2] CA reactions indicate that the LA catalyst changes completely the mechanism of these processes. Indeed, for the [2+2] CA reaction, the process changes from one step to stepwise mechanism, while for the [4+2] CA reaction, the mechanism becomes highly asynchronous, since the difference between the lengths of the new forming bonds is 1.07 and 1.19 Å for **TS1mn-c** and **TS1mx-c**, respectively. For the LA-catalysed [4+2] process, the BO's values of the C1–C5 and C4–C6 new forming bonds confirm the above asynchronous remarks in which the C1–C5 bond formation is more advanced than the C4–C6 one.

The values of GEDT, which its flux takes place from **MPA** to the electrophilically activated LA-**MA** complex, are 0.29e (**TS1mn-c**) and 0.33e (**TS1mn-c**). The GEDT found in these TSs accounts for the polar character of this LA-catalysed CA reaction. Therefore, the LA catalyst increases the polar character of these CA reactions, explaining the decrease of the activation energies of these processes.

ELF topological analysis

ELF characterisation of the electronic structure of reagents

An attractive procedure that has given us a direct link between the distribution of electron density and the chemical structure is the quantum chemical topological analysis of ELF established by Becke and Edgecombe [39]. Several studies can be found in the literature which applies ELF topological analysis for different chemical systems can be found in the literature [56–58].

ELF localisation domains and their attractor positions, together with the most representative valence basin populations of **MPA**, **MA** and **MA**-LA are shown in Fig. 5. Recent studies based on Molecular Electron Density Theory (MEDT) [59] indicate that the electronic structure of a molecules has a very good correlation with its reactivity [60–62].

The ELF analysis of **MA** structure indicates the presence of the following basins: two V(C5,C6) and V′(C5,C6) disynaptic with a population of 1.72e for each one and a disynaptic V(C,O) integrating an electron population of 2.38e. In addition, two mono synaptic basins V(O) and V′(O) integrating 2.68 and 2.63e, respectively, corresponding to non-bonding regions within the context of ELF. For the **LA-MA** complex,

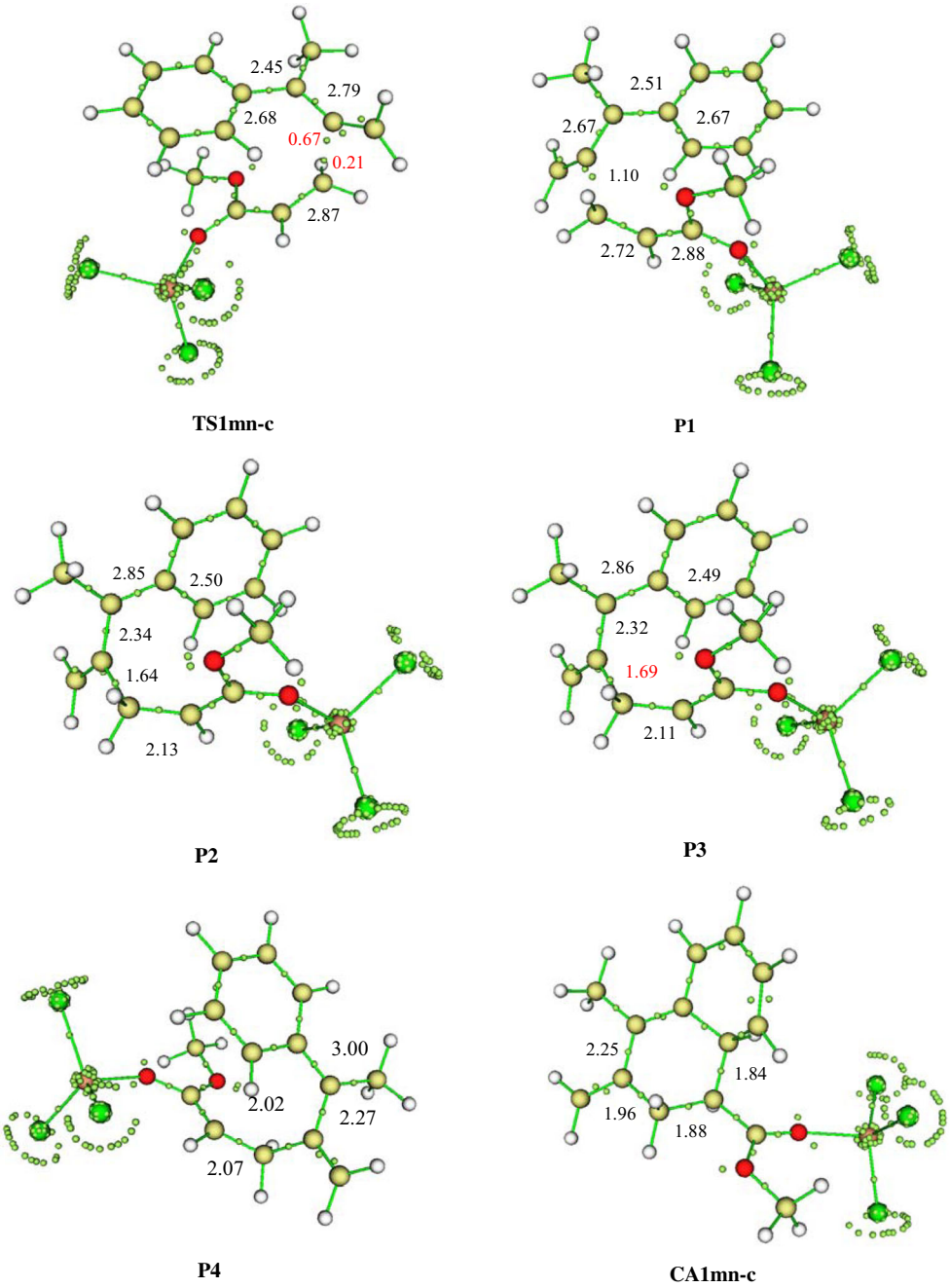

Fig. 6 ELF basins attractor's positions of relevant points of the IRC path together with the populations of the relevant basins along the most favourable meta/endo CA reaction pathway associated with the *meta-endo* [4+2] CA reaction of **MPA** with **MA-LA**

ELF topological analysis shows the presence of the same basins with a remarkable change of electron population. Indeed, the population of two V(C5,C6) and V′(C5,C6) disynaptic decreases to become integrating 1.67e for each one. The population of the disynaptic V(C,O) basin also decreases to 2.00e and contrariwise the population of the non-bonding regions V(O) and V′(O) becomes integrating 2.95 and 2.74e, respectively. These changes of electron population of the most relevant basins indicate that the addition of Lewis acid to **MA** pulls electron density towards him and consequently empty the reactive region of **MA** and enhance its reactivity towards a nucleophilic attack, which explain clearly the high electrophilicity of **MA**-LA and the low activation energies of the corresponding CA reactions.

For the **MPA** structure, ELF topological analysis of the most relevant basins corresponding to the reactive regions indicates the presence of a two disynaptic basins V(C1,C2) and V′(C1,C2) integrating a total population of 3.78e, whereas, the bonding region C3–C4 shows only one disynaptic basin V(C3,C4) integrating 2.72e. Consequently, ELF topological analysis of **MPA** structure reveals that C1–C2 bonding region is more reactive than the C3–C4 one, in greet agreement with the nucleophilic Parr function analysis (see above).

Table 10 ELF valence basin populations of the selected points of the IRC involved in the formation of the C1–C5 and C4–C6 single bonds along the *meta-endo* [4+2] CA reaction of **MPA** with **MA**-**LA**. Distances are given in angstroms, Å, and GEDT values and electron populations in average number of electrons, e

Points	TS1mn-c	P1	P2	P3	P4	CA1mn-c
d(C1–C5)	2.01	1.92	1.64	1.61	1.57	1.52
d(C4–C6)	3.08	3.07	3.01	2.97	2.60	1.56
GEDT	0.288	0.333	0.451	0.46	0.43	0.05
V(C3,C4)	2.68	2.67	2.51	2.49	2.44	1.98
V(C1,C2)	2.79	2.67	2.35	2.32	2.27	2.25
V(C5,C6)	2.87	2.72	2.13	2.11	2.07	1.88
V(C1)	0.67	–	–	–	–	–
V(C5)	0.21	–	–	–	–	–
V(C1,C5)	–	1.10	1.64	1.69	1.80	1.96
V(C4)	–	–	–		–	–
V(C6)	–	–	–	–	2.02	–
V(C4,C6)	–	–	–	–	–	1.84

ELF topological analysis of the formation processes of the new C–C single bonds

In order to carry out an in-depth study of the mechanism of these CA reactions catalysed by $AlCl_3$ and to characterise the nature of the formation of the new single bonds, an ELF topological analysis of some selected points on the IRC path of the most favourable *meta-endo* [4+2] reactive channel was performed. The electronic populations of the most significant valence basins with the corresponding ELF basin attractor positions of the selected structures of the IRC are shown in Fig. 6. ELF valence basin populations of these selected points corresponding to the formation of the C1–C5 and C4–C6 single bonds along the *meta-endo* [4+2] CA reaction of **MPA** with **MA**-**LA**, with distances and GEDT values are gathered in Table 10.

At **TS1mn-c**, some topological changes are observed on the reactive regions with respect to the structure of the ground state of both frameworks, which are the two new V(C1) and V(C5) monosynaptic basins, integrating 0.61 and 0.21e, respectively. These topological changes allow concluding that the initial C1–C2 and C5–C6 double bonds are already broken before TS point leading to the formation of a C1 and C5 pseudoradical centres necessary for the formation of the single new forming bond C1–C5.

At **P1**, a second remarkable change on the bonding region is the cohesion of the C1 and C5 pseudoradical centres in a new V(C1,C5) disynaptic basin with a population of 1.10e, indicating the beginning of the formation of the first C1–C5 single bond. In parallel, the population of the two disynaptic basins V(C1,C2) and V(C5,C6) keeps on decreasing to reach 2.67 and 2.72, respectively.

At **P2**, the most remarkable change is related to the slight increase of the population of the new V(C1,C5) disynaptic basin by 0.54e to become integrating 1.64 e. Decreasing of electron density is a consequence of the displacement of electron density from **MPA** over C1 atom. The population decreases of V(C1,C2) and V(C4,C5) disynaptic basins continue at this point and contributing to the increase of the population of the new forming bond C1–C5.

At **P3**, analysis of the bonding region's basins indicates that no significant change was performed, only a slightly increase of the population of the V(C1,C5) disynaptic basin towards integrating 1.69e and decreasing of the V(C1,C2) and V(C4,C5) disynaptic's population towards 2.32 and 2.11e, respectively.

At **P4**, which it considers the last step before the full formation of the cycloadduct, the most remarkable change is the formation of a two monosynaptic basins V(C4) et V′(C4) integrating a total population 2.02e, account for the zwitterionic character of this stage and the beginning of the formation of the second C4–C6 single bond.

Finally at **CA1mn-c**, the apparition of a V(C4,C6) disynaptic basin integrating 1.84 e indicates that the second C4–C6 single bond is formed at this point, which suggest the formation delay of the second new bond until the last stage of this CA reaction, while the population of the V(C1,C5) disynaptic basin related to the C1–C5 single bond decrease slightly to 1.96 e.

This ELF topological analysis associated to the formation of the C1–C5 and C4–C6 single reveals that the LA-catalysed [4+2] CA reaction takes place through a two-stage one-step mechanism [63] in which the formation of the second C4–C6 single bond begins when the first C1–C5 single bond is completely formed. The first C1–C5 single bond is formed through a formation of pseudo-diradical intermediate, while the second C4–C6 one is formed by a zwittérionic mechanism at the last stage of the reaction. These results account that the molecular mechanism is non-concerted.

Conclusion

The nature of mechanism, the regio-and the steroselectivities of the non-catalysed and $AlCl_3$ Lewis acid catalysed completive [4+2]/[2+2] CA reaction between **MPA** and **MA** to yield predominately the *meta* [4+2] regioisomers have been studied by MEDT using quantum chemical DFT methods at the B3LYP/6-31G(d) computational level.

Analysis of the global reactivity indices allows classifying **MPA** as a strong nucleophile and **MA** as a moderate electrophile. The coordination of the $AlCl_3$ catalyst with **MA** increases its reactivity to become a strong electrophile, which leading to enhance dramatically the polar character of the corresponding CA reaction, in clear agreement with the obtained high GEDT and the low activation energies. Analysis of

the Parr functions explain well the total regioselectivity experimentally found in this cycloadditions.

In non-catalysed gas phase or in a solution, these competitive CA reactions preceded via an asynchronous mechanism favour the formation of the *meta* regioisomers kinetically and thermodynamically. The obtained low values of GEDT accounts for a low polar character of these CA reactions and well explaining the high activation energies. The most notice of the inclusion of dichloromethane effects is the slight increases of the activation energies and the decreases the exothermic character of these CA reactions.

Formation of MA-LA complex decreases the activation energies and increases the polar character of these CA reactions, leading to formation of a mixture of both [4+2] and [2+2] *meta* regioisomers, in which the *meta* [4+2] regioisomers is the major cycloadducts, in agreement with experimental data. The dichloromethane solvent effect has no influence on the selectivity but it increases slightly the activation energies. The analysis of activation Gibbs free energies reveals that the *meta* cycloadducts are favoured kinetically.

The LA-catalysed [4+2] CA reaction takes place via a highly asynchronous mechanism, while for the LA [2+2] CA reaction become proceeds through a stepwise mechanism.

ELF topological analysis of **MA** and **MA-LA** complex shows that the coordination of $AlCl_3$ catalyst to **MA** enhances its reactivity towards a nucleophilic attack on the reactive region by moving the electron density of the C5=C6 double bond towards the oxygen atom of carbonyl function (C=O). The ELF topological analysis of **MPA** structure indicates that the C1=C2 reactive region is characterised by a high electron density than the C3=C4 one explaining its precedence in reactivity.

ELF topological analysis of the formation of the two new single bonds along the most favourable [4+2] *meta/endo* reaction pathway indicates that the formation of the first C1–C5 single bond takes place by coupling a C and C of C1 and C5 pseudoradical centres at the first stages of the reaction, while, the second C4–C6 single bond formed by the donation of a non-bonding electron density of the C5 carbon atom of ethylene fragment, which developed at the last stage of the reaction, account for a zwitterionic mechanism. The two-stage one-step mechanism of these CA reactions indicates that this mechanism is non-concerted.

Compliance with ethical standards

Conflict of interest The authors declare that they have no conflict of interest.

References

1. W. Carruthers, Cycloaddition reactions in organic synthesis, Pergamon, Oxford, 1990
2. Fringuelli F, Taticchi A (1990) Dienes in the Diels–Alder reaction. Wiley, New York
3. Paquette LA (1991) In comprehensive organic synthesis, vol 5. PergamonPress, Oxford
4. Hayashi Y, Narasaka K (1989). Chem Lett:793
5. Narasaka K, Hayashi K, Hayashi Y (1994). Tetrahedron 50:4529
6. Takenaka Y, Ito H, Hasegawa M, Iguchi K (2006). Tetrahedron 62: 3380
7. Mitsudo TA, Naruse H, Kondo T, Ozaki Y, Watanabe Y (1994). Angew Chem Int Ed 33:580–581
8. Wei D, Zhu Y, Zhang C, Sun D, Zhang W, Tang M (2011). J Mol Catal A Chem 334:108–115
9. Nacereddine AK, Yahia W, Sobhi C, Djerourou A (2012). Tetrahedron Lett 53:5784
10. Bouacha S, Nacereddine AK, Djerourou A (2013). Tetrahedron Lett 54:4030
11. Jasiński R (2016). Reac Kinet Mech Cat 119:49
12. Huisgen R (1980). Pure Appl Chem 52:2283
13. Firestone RA (1996). Tetrahedron 52(46):14459–14468
14. Singleton DA, Schulmeier BE, Hang C, Thomas AA, Leung SW, Merrigan SR (2001). Tetrahedron 57(24):5149–5160
15. Jasiński R, Kubik M, Łapczuk-Krygier A, Kącka A, Dresler E, Boguszewska-Czubara A (2014). React Kinet Mech Catal 113: 333–345
16. Jasiński R (2014). Comput Theor Chem 1046:93–98
17. Jasiński R (2017). J Mol Graph Model 75:55–61
18. Conner ML, Brown MK (2016). Tetrahedron 72:3759
19. Bartlett PD, Wallbillich G, Wingrove AS, Swenton JS, Montgomery LK, Kramer BD (1968). J Am Chem Soc 90(8): 2049–2056
20. Nacereddine K, Yahia W, Bouacha S, Djerourou A (2010). Tetrahedron Lett 51:2617
21. Yahia W, Khorief Nacereddine A, Liacha M, Djerourou A (2018). Int J Quantum Chem 118:e25540
22. Sobhi C, Nacereddine AK, Djerourou A, Aurell MJ, Domingo LR (2012). Tetrahedron 68:8457
23. Yahia W, Nacereddine AK, Liacha M (2014). Prog React Kinet Mec 39:365
24. Chafaa F, Hellel D, Nacereddine AK, Djerourou A (2016). Tetrahedron Lett 57:67–70
25. Dennington, R.; Keith, T.; Millam, J. (2009) GaussView, version 5; Semichem Inc.: Shawnee Mission, KS
26. Frisch MJ et al (2009) Gaussian 09, revision A.02. Gaussian Inc. Wallingford
27. Lee C, Yang W, Parr RG (1988). Phys Rev B 37:785
28. Becke AD (1993). J Chem Phys 98:5648
29. Hehre WJ, Radom L, Schleyer PVR, Pople JA (1986) Ab initio molecular orbital theory. Wiley, New York
30. Tomasi J, Persico M (1994). Chem Rev 94:2027
31. Simkin BY, Sheikhet I (1995) Quantum chemical and statistical theory of solutions a computational approach. Ellis Horwood, London
32. Cances E, Mennucci B, Tomasi J (1997). J Chem Phys 107:3032
33. Cossi M, Barone V, Cammi R, Tomasi J (1996). Chem Phys Lett 255:327
34. Barone V, Cossi M, Tomasi J (1998). J Comput Chem 19:404
35. Becke AD (1993). J Chem Phys 98:5648
36. Becke AD, Weinstock RB, Weinhold F (1985). J Chem Phys 83: 735
37. Reed AE, Curtiss LA, Weinhold F (1988). Chem Rev 88:899
38. Becke AD, Edgecombe KE (1990). J. Chem Phys 92:5397–5403
39. Lu T, Chen F (2012). J Comput Chem 33:580–592
40. Parr RG, Von Szentpaly L, Liu S (1999). J Am Chem Soc 121: 1922–1924
41. Parr RG, Szentpaly LV, Liu S (1983). J Am Chem Soc 105:7512–7516

42. Parr RG, Yang W (1989) Density functional theory of atoms and molecules. Oxford University Press, New York
43. Jaramillo P, Domingo LR, Chamorro E, Pérez P (2008). J. Mol. Struct. THEOCHEM 865:68–76
44. Kohn W, Sham LJ (1965). Phys Rev 140:1133–1138
45. Domingo LR, Pérez P, Sáez JA (2013). RSC Adv 3:1486–1494
46. Domingo LR, Aurell MJ, Pérez P, Contreras R (2002). Tetrahedron 58:4417
47. Domingo LR, Pérez P (2013). Org Biomol Chem 11:4350
48. Domingo LR, Emamian SR (2014). Tetrahedron 70:1267
49. Nacereddine AK, Layeb H, Chafaa F, Yahia W, Djerourou A, Domingo LR (2015). RSC Adv 5:64098
50. Chafaa F, Hellel D, Nacereddine AK, Djerourou A (2016). Mol Phys 114:663
51. Hellel D, Chafaa F, Nacereddine AK, Djerourou A, Vrancken E (2017). RSC Adv 7:30128
52. Ríos-Gutiérrez M, Chafaa F, Nacereddine AK, Djerourou A, Domingo LR (2016). J Mol Graphics Modell 70:296–304
53. Wiberg KB (1968). Tetrahedron 24:1083
54. Domingo LR (2014). RSC Adv 4:32415
55. Berski S, Gordon AJ (2012). Chem Phys Lett 525–526:24–31
56. Durlak P, Mierzwicki K, Latajka Z, Ratajczak H (2010). J Mol Struct 976:392–396
57. Hernández-Trujillo J, García-Cruz I, Martínez-Magadán JM (2005). Chem Phys 308:181–192
58. Domingo LR (2016). Molecules 21:1319
59. Emamian, S., Lu, T., Domingo, L. R., Saremi, L. H., Ríos-Gutiérrez, M. (2018). Chemical physics
60. Nasri L, Ríos-Gutiérrez M, Nacereddine AK, Djerourou A, Domingo LR (2017). Theor Chem Acc 136(104)
61. Ríos-Gutiérrez M, Nasri L, Khorief Nacereddine A, Djerourou A, Domingo LR (2018). J Phys Org Chem:e3830
62. Domingo LR, Ríos-Gutiérrez M, Pérez P (2018). J Org Chem
63. Domingo LR, Saéz JA, Zaragozá RJ, Arnó M (2008). J Org Chem 73:8791